

BIOMECHANICS

Biomimetic fracture model of lizard tail autotomy

Navajit S Baban¹, Ajymurat Orozaliev¹, Sebastian Kirchof², Christopher J Stubbs³, Yong-Ak Song^{1,4,5*}

Lizard tail autotomy is an antipredator strategy consisting of sturdy attachment at regular times but quick detachment during need. We propose a biomimetic fracture model of lizard tail autotomy using multiscale hierarchical structures. The structures consist of uniformly distributed micropillars with nanoporous tops, which recapitulate the high-density mushroom-shaped microstructures found on the lizard tail's muscle fracture plane. The biomimetic experiments showed adhesion enhancement when combining nanoporous interfacial surfaces with flexible micropillars in tensile and peel modes. The fracture modeling identified micro- and nanostructure-based toughening mechanisms as the critical factor. Under wet conditions, capillarity-assisted energy dissipation pertaining to liquid-filled microgaps and nanopores further increased the adhesion performance. This research presents insights on lizard tail autotomy and provides new biomimetic ideas to solve adhesion problems.

For millions of years, the constant struggle for survival has driven lizards to evolve a defense mechanism known as tail or caudal autotomy (1, 2). This autotomy has a seemingly paradoxical nature: sturdy attachment at normal times but quick detachment during need. As an explanation of tail autotomy, previous studies have reported the segmented anatomy of the lizard tail with functional fracture planes (3, 4) in skeletal

muscles throughout the postpygal vertebrae (for details, see supplementary text 1). The fracture planes consist of the bulged-out distal ends of muscle fibers arranged as highly dense, mushroom-shaped micropillars (separated by connective tissue) (3, 4) with a role in autotomy that is still not understood quantitatively.

From an engineering perspective, a typical fracture plane would make the tail overly vulnerable to fracture, even in situations that are

not life threatening. In reality, the tail remains sturdily and faithfully connected to the body part, quickly detaching only when the lizard wills it. Simplistic fracture models of lizard tail autotomy cannot resolve the tail's attachment's seemingly paradoxical nature. A proteomic study (3) on the fluid that was released after Tokay gecko tail autotomy revealed an absence of any protein-breaking chemicals, thus suggesting a mechanical fracture problem. To understand the biophysics of lizard tail autotomy, we analyzed the fracture plane connections of three different lizard species: *Hemidactylus flaviviridis* (Gekkonidae), *Cyrtopodion scabrum* (Gekkonidae), and *Acanthodactylus schmidtii* (Lacertidae).

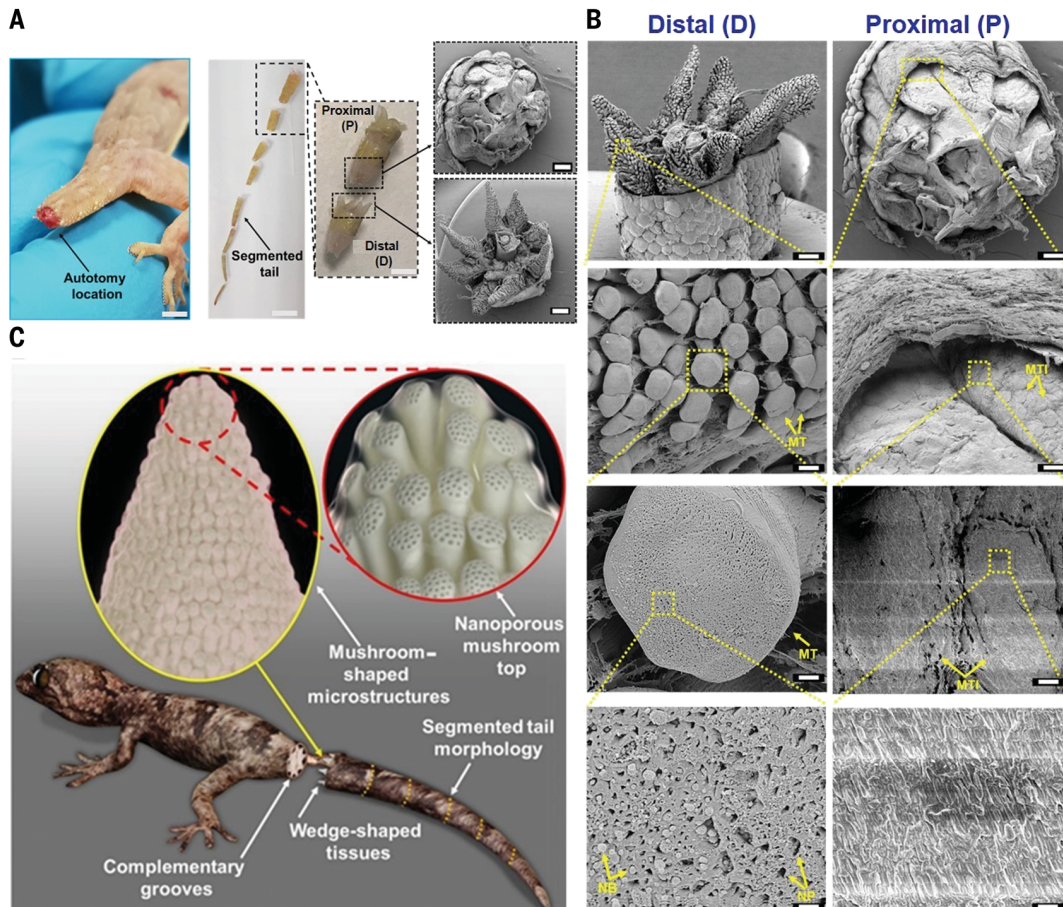
Fig. 1A shows the autotomy location in the *H. flaviviridis* individual's tail and illustrates the segmented nature of the tail connected

Fig. 1. Scanning electron microscope (SEM) image of the autotomized interface of an

H. flaviviridis tail. (A) Autotomized tail location (scale bar, 1.5 cm). Segmented tail morphology (scale bar, 1 cm) shows region P, representing the proximal part of the tail, and region D, representing the distal part (scale bar, 0.5 cm), in a plug-and-socket type assembly (scale bar, 1 mm).

(B) SEM of the distal (D) part showing the wedge-shaped tissues with highly dense mushroom-shaped microstructures (scale bar, 1 mm). The enlarged portion shows the mushroom-shaped micropillared arrangement (scale bar, 100 μ m) with the single mushroom top indicated as MT (scale bar, 10 μ m) containing the nanopores (NP) and nanobeads (NB) (scale bar, 1 μ m). SEM of region P (scale bar, 1 mm) shows the corresponding MT imprints indicated as MTI (scale bar, 100 μ m). The single MTI (scale bar, 10 μ m) shows a planar topology (scale bar, 1 μ m).

(C) Hypothesized model of the lizard tail interface between two complementary segments before fracture, consisting of micropillared nanoporous top connections at the wedge-shaped tissue faces.



¹Division of Engineering, New York University Abu Dhabi, Abu Dhabi, United Arab Emirates. ²Division of Science, New York University Abu Dhabi, Abu Dhabi, United Arab Emirates. ³Gildart Haase School of Computer Sciences and Engineering, Fairleigh Dickinson University, Teaneck, NJ 07666, USA. ⁴Department of Chemical and Biomolecular Engineering, Tandon School of Engineering, New York University, New York, NY 11201, USA. ⁵Department of Biomedical Engineering, Tandon School of Engineering, New York University, New York, NY 11201, USA.

*Corresponding author. Email: rafael.song@nyu.edu

through a “plug-and-socket” sort assembly. The distal part contains eight (two ventral, four lateral, and two dorsal) circumferentially arranged wedge-shaped muscle bundles, whereas the proximal part encloses the corresponding complementary grooves or pockets lined with layers of connective tissue (myosepta). Fig. 1B shows the high-density mushroom-shaped micropillars (muscle fibers with dilated termini) on the wedge-shaped muscle bundle and the complementary pockets where the wedges remained inserted before fracture. Microcomputer tomography of the fractured tail (*H. flaviviridis* individual) showed fragmented intravertebral fracture planes located in close proximity to the wedge-shaped muscle fracture planes (see supplementary text 2). The enlarged portions within Fig. 1B show the associated mushroom top with dense nanopores and scanty nanobeads constituting the interface. The magnified view of the complementary pockets shows the planar mushroom top imprints in the myoseptum resulting from its surface contact-based attachment with the mushroom top in vivo. These surface imprints implied that the mushroom tops were not penetrating the proximal part, as would be the case for stronger tail attachment. Instead, the lizard has adopted a different strategy for tail attachment at the interface composed of the surface contact-based attachment with microscale and nanoscale discontinuities. Thus, we hypothesize a model of how the distal tail section could have been attached to the proximal one before fracture, in which mushroom-shaped microstructures contact the opposite surface with their nanoporous tops, as schematically illustrated in Fig. 1C.

These multiscale hierarchical features correlated with design strategies extensively found in nature (for examples, see supplementary text 3) that imply toughening mechanisms associated with micro- and nanoscale structural features. The high-speed video analysis showed that the tail's bending actuated the fracture (movies S3 and S4 and supplementary text 4). By contrast, the tensile stretching of the tail showed no fracture at all (Fig. 2). Moreover, on the basis of the *H. flaviviridis* specimens analyzed ($n = 7$), it was also confirmed that the tail should be grasped at least a short distance distal to the autotomy plane. This would provide a sufficient pivot length about which the muscles can favorably act. For *A. schmidtii*, the shorter pivot distance required more force to induce the fracture (movie S5 and S6).

To support our hypothesis, we built a biomimetic model using polydimethylsiloxane micropillars with nanoporous tops in two different height ranges: 1.75 to 30 μm as low-aspect-ratio micropillars and 30 to 100 μm as high-aspect-ratio micropillars (Fig. 3, A and B). For both the low- and high-aspect-ratio micropillars, the results in Fig. 3, C to H and I to N (summarized in table S1), show that adhesion energy and peak force significantly decreased in peel mode (see experimental details in supplementary text 5), demonstrating the fracture's mode-dependent vulnerability. The difference in mode-dependent results can be explained by the equal load sharing of the micropillars (5), which was quantified by comparing the associated characteristic stress decay lengths (6, 7). We recorded a 17-fold difference between the modes (see the “Equal load sharing calculation” section in supplementary text 5). The mode-dependent find-

ings correlated with the experimental results of the high-speed video analysis showing a facile fracture in the bending mode.

Within each mode, a significant increase in adhesion energy and peak force was obtained at nanoporous top surfaces, thus validating the role of micropillared nanoporous interface in improving the adhesion performance. The combined use of micropillared interface with nanoporous top showed a significant adhesion enhancement for both low-aspect ratio micropillars (maximally, 7.9-fold in the tensile mode and 4.5-fold in the peel mode) and high-aspect ratio micropillars (maximally, 14.8-fold in the tensile mode and 14-fold in the peel mode) compared with the plain unstructured interface. The enhancement effect of the nanoporous interface can specifically be filtered out by comparing the plain top and nanoporous top pillars' results, in which a significant adhesion increment was recorded for both the low-aspect-ratio micropillar (4.8-fold in the tensile mode and 2.5-fold in the peel mode) and the high-aspect-ratio micropillar (1.4-fold in the tensile mode and 2.1-fold in the peel mode).

The hierarchical toughening can be explained as follows. First, the nanoporous-assisted contact on top of the micropillars exerts a crack-arresting effect that can be explained by the crack initiation at multiple discontinuities plus the coplanar Cook-Gordon mechanism (7, 8) that imparted repulsive stress interactions between the vicinal coplanar cracks (8, 9) during propagation. This greatly contributed toward the intrinsic (10) fracture toughening mechanism at the interface. Furthermore, multiple nanolevel discontinuity-associated intermittent crack propagations induced a coplanar Lake-Thomas (8) effect that dissipated energy similar to bond rupturing in soft elastomer chains. Second, the phenomenon of flaw insensitiveness (5) caused by micropillar-based contact-splitting phenomena also contributed to the increasing adhesion through extrinsic (10) toughening in tandem with the nanopore-induced intrinsic toughening. Last, as the micropillars' height increased, a considerably large amount of strain energy was absorbed by the flexible micropillars, improving the extrinsic toughening further (see the “Flaw insensitivity” and “Effect of micropillar height” sections in supplementary text 5). For the high-aspect-ratio micropillars, the 100- μm -high micropillars that closely resembled the mushroom-like microstructures in terms of their aspect ratio showed the highest adhesion energy and peak forces.

We also evaluated the effect of strain rate, prestress, and wet conditions (see supplementary text 6) and found improvement in adhesion performance in all cases. The adhesion performance improvement in wet conditions was attributed to the combined effect of microscale and nanoscale liquid bridges (11) in dissipating elastic energy, plus the spatially varying

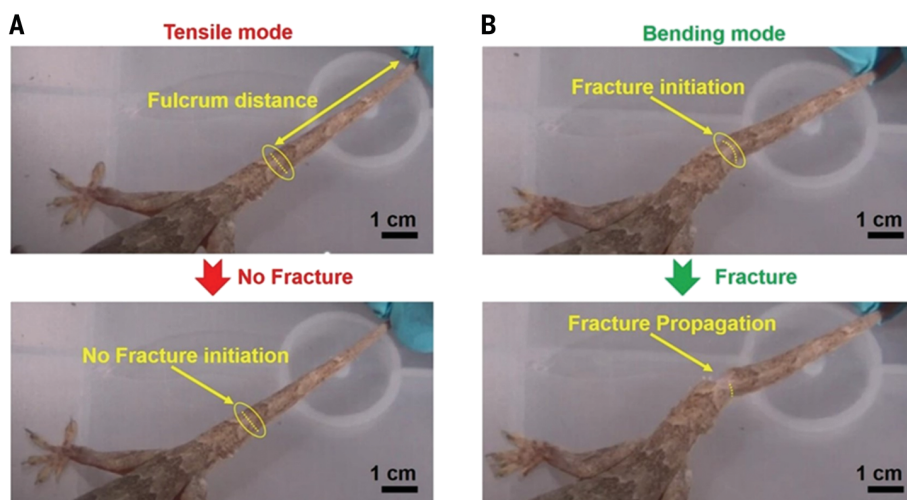


Fig. 2. High-speed analysis of tail autotomy. (A) Tensile mode, in which the tail was in the fully stretched condition with the fulcrum distance between the fracture plane and the grasp point. No fracture initiation was observed for the tensile stretching mode. (B) Bending mode, in which the tail was in the fully stretched condition showing fracture initiation. Catastrophic fracture propagation was observed after the fracture initiation in the bending mode.

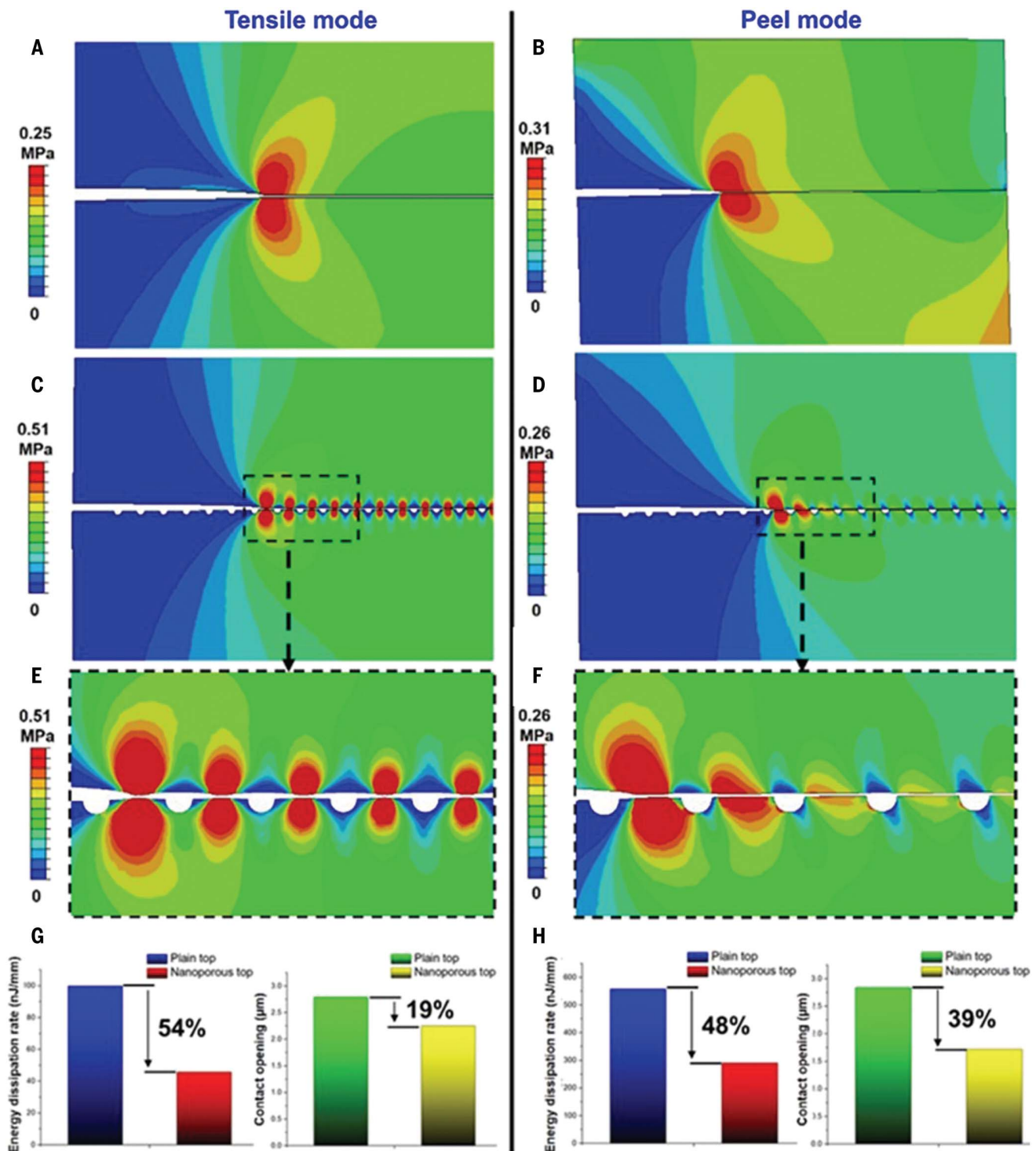


Fig. 4. Computational fracture modeling of a plain top versus nanoporous micropillar interface. (A to D) Maximum principal stress contour plots for the plain top micropillar (1.75 μm in height) in the tensile mode (A) and in the peel mode (B) and for the nanoporous top micropillar in the tensile mode (C)

and in the peel mode (D). (E and F) Stress field interaction as a result of the coplanar Cook-Gordon mechanism in the tensile mode (E) and in the peel mode (F). (G and H) Strain energy dissipation rate and contact opening comparison in the tensile mode (G) and in the peel mode (H).

with nanoporous top surfaces in tail autotomy. These micropillars and nanopores establish interfacial connections along the tail fracture planes that are exposed to higher vulnerability in bending mode than in tensile mode. How-

ever, within each mode, the connections showed toughening mechanisms with nanoporous top micropillars that helped the tail avoid undue breakage. The intrinsic toughening mechanisms were composed of nanolevel crack discontinu-

ities that assisted the coplanar version of the Cook-Gordon mechanism and the Lake-Thomas effect. Furthermore, the increased height of micropillars, as well as the flaw insensitivity caused by microlevel discontinuities, contributed

to the extrinsic toughening mechanisms. In wet conditions, microscale and nanoscale liquid bridges facilitated capillary-assisted and suction-based energy dissipation. This, along with the toughening mechanisms associated with direct solid-solid contact, improved the adhesion performance. Using this multiscale interfacial strategy, the lizard carefully balances attachment and detachment, achieving the “just right” connection in its tail that is neither too weak nor too strong for its best chance of survival.

REFERENCES AND NOTES

1. E. N. N. Arnold, *J. Nat. Hist.* **18**, 127–169 (1984).
2. P. W. Bateman, P. A. Fleming, *J. Zool.* **277**, 1–14 (2009).
3. K. W. Sanggaard *et al.*, *PLOS ONE* **7**, e51803 (2012).
4. T. H. Araújo, F. P. de Faria, E. Katchburian, E. F. Haapalainen, *Acta Zool.* **91**, 440–446 (2010).
5. A. Jagota, C. Y. Hui, *Mater. Sci. Eng. Rep.* **72**, 253–292 (2011).
6. D. A. Dillard, B. Mukherjee, P. Karnal, R. C. Batra, J. Frechette, *Soft Matter* **14**, 3669–3683 (2018).
7. N. S. Baban, A. Orozaliev, C. J. Stubbs, Y. A. Song, *Phys. Rev. E* **102**, 012801 (2020).
8. J. Y. Chung, M. K. Chaudhury, *J. R. Soc. Interface* **2**, 55–61 (2005).
9. J. C. Hill *et al.*, *Int. J. Fract.* **119**, 365–386 (2003).
10. R. O. Ritchie, *Nat. Mater.* **10**, 817–822 (2011).
11. Q. Liu *et al.*, *ACS Appl. Mater. Interfaces* **12**, 19116–19122 (2020).
12. A. Ghatak, *Phys. Rev. E Stat. Nonlin. Soft Matter Phys.* **89**, 032407 (2014).

ACKNOWLEDGMENTS

We thank A. Bauer for helpful discussions on the biology of tail autotomy; P. Salmon from Bruker Belgium for CT scanning the lizard tail; the NYU Abu Dhabi graduate office for providing N.S.B. with a Global Ph.D. Fellowship; and the NYU Abu Dhabi Core Technology Platform, especially R. Pasricha and J. Weston, for providing us access and help with the SEM study. **Funding:** This work was supported by an annual research grant provided by NYU Abu Dhabi. **Author contribution:** N.S.B. conducted SEM analysis, high-speed videography and analysis, biomimetic sample preparation, characterization and results analysis, and finite element simulations. A.O. fabricated masters for the biomimetic model. S.K. was in charge of lizard biology and evolution and assisted in capturing, identifying, and performing high-speed

videography of autotomy. C.J.S. assisted and checked finite element simulations. Y.A.S. planned, guided, and coordinated the project. All authors contributed to the writing of the manuscript. **Competing interests:** The authors declare no competing interests. S.K. is also affiliated with the Museum für Naturkunde Berlin, Leibniz Institute for Evolution and Biodiversity Science, Berlin (Germany) as a guest researcher, but this affiliation has no competing interests for the current paper. **Data and materials availability:** All data and materials are available in the main manuscript or the supplementary materials.

SUPPLEMENTARY MATERIALS

science.org/doi/10.1126/science.abh1614
Materials and Methods
Supplementary Text 1 to 7
Figs. S1 to S32
Tables S1 to S4
References (13–31)
Movies S1 to S12

Accepted 20 December 2021

21 February 2022; resubmitted 5 November 2021

Accepted 20 December 2021

10.1126/science.abh1614